Journal of Nuclear Materials 458 (2015) 233–239

Contents lists available at ScienceDirect

Journal of Nuclear Materials

journal homepage: www.elsevier.com/locate/jnucmat

# Hydrogen diffusion and trapping in nanocrystalline tungsten

P.M. Piaggi [a], E.M. Bringa [b,c,*], R.C. Pasianot [a,c,d], N. Gordillo [e], M. Panizo-Laiz [e], J. del Río [f], C. Gómez de Castro [g], R. Gonzalez-Arrabal [e]

[a] Instituto Sabato, UNSAM/CNEA, Avda. Gral. Paz 1499, 1650 San Martín, Argentina
[b] Facultad de Ciencias Exactas y Naturales, Universidad Nacional de Cuyo, Mendoza 5500, Argentina
[c] CONICET, Avda. Rivadavia 1917, 1033 Buenos Aires, Argentina
[d] CAC-CNEA, Gerencia de Materiales, Avda. Gral. Paz 1499, 1650 San Martín, Argentina
[e] Instituto de Fusión Nuclear, Universidad Politécnica de Madrid, C/ José Gutiérrez Abascal 2, E-28006 Madrid, Spain
[f] Departamento de Física de Materiales, Facultad de CC. Físicas, Universidad Complutense de Madrid, Ciudad Universitaria s/n, E-28040 Madrid, Spain
[g] Departamento de Física de Materiales, Facultad de CC. Químicas, Universidad Complutense de Madrid, Ciudad Universitaria s/n, E-28040 Madrid, Spain

ARTICLE INFO

*Article history:*
Received 26 August 2014
Accepted 15 December 2014
Available online 24 December 2014

ABSTRACT

The hydrogen behavior in nanocrystalline W (ncW) samples with grain size of 5 and 10 nm is studied using Molecular Dynamics (MD) with a bond order potential (BOP) for the W–H system. The dependence of the hydrogen diffusion coefficient on grain size (5 and 10 nm) and hydrogen concentration (0.1 at.% < [H] < 10.0 at.%) is calculated. These data show that in all cases the hydrogen diffusion coefficient is lower for ncW than for coarse-grained samples. Trapping energies of grain boundaries are estimated and a broad distribution roughly centered at the vacancy trapping energy is found. Hydrogen diffusion results are interpreted within the trapping model by Kirchheim for nanocrystalline materials. The H–H interaction is evaluated and the possible formation of $H_2$ is disregarded for the conditions in these simulations. Hydrogen segregation and trapping in grain boundaries for ncW is discussed, including extrapolations for micron-sized polycrystals.



## 1. Introduction

One of the challenges in designing future nuclear power plants is to develop materials capable of enduring the hostile environment of a fusion reactor. Because of its properties (i.e. low sputtering yield, low-activation, high melting point, high thermal conductivity and low thermal expansion), tungsten is one of the most attractive materials proposed as plasma facing material (PFM) in nuclear fusion reactors, both in the magnetic as well as in the inertial confinement approach [1–3]. However, some limitations have been identified that must be remedied in order to fulfill specifications: (i) it has a high ductile-to-brittle transition temperature (DBTT), which is a consequence of the non-planar screw dislocations core and their high activation energies for glide and (ii) it suffers from surface blistering and exfoliation when irradiated with hydrogen isotopes above certain fluence [4], which is unacceptable for a PFM. The main reason for this surface deterioration is related to the accumulation of gases and the formation of bubbles which can easily grow, becoming overpressurised.

Using nanocrystalline materials has been proposed as a solution to both issues [3,5]. On one hand, there is evidence that ultra-fine grained tungsten exhibits a lower DBTT [6] since deformation mechanisms are grain size dependent [7]. On the other hand, under certain conditions, nanostructured materials have been demonstrated to be self-healing materials. This is because, at and above room temperature, grain boundaries (GBs) behave as annihilation centers for Frenkel pairs [8,9] and as pinning centers for light species [10,11]. These two facts may delay (shift to larger fluences) the formation of overpressurized bubbles and, therefore, delay surface blistering and exfoliation. Because of this, in order to asses the capabilities of nanocrystalline tungsten (ncW) as PFM, the understanding of the influence of the GBs in the diffusion and trapping mechanisms of hydrogen in ncW is of primordial importance.

Nevertheless, so far the behavior of H in nanostructured materials has not been sufficiently studied. Hitherto, from the experimental point of view, most studies were devoted to characterize hydrogen and hydrogen-isotopes behavior in polycrystalline W. Those experiments evidence that implanted hydrogen-isotopes are trapped in native defects with trapping energies between 0.5 and 1.5 eV [12,13]. However, since real samples may contain a large diversity of native defects, i.e. GBs, dislocations, impurities, etc., from these data the role of GBs in hydrogen trapping cannot

* Corresponding author at: Facultad de Ciencias Exactas y Naturales, Universidad Nacional de Cuyo, Mendoza 5500, Argentina.
*E-mail address:* ebringa@yahoo.com (E.M. Bringa).

http://dx.doi.org/10.1016/j.jnucmat.2014.12.069
0022-3115/

be directly assessed. On the other hand, computer simulations carried out so far were oriented to study hydrogen diffusion and trapping in GBs using bicrystals [14–16], and thus dealt with hydrogen behavior in very ideal systems. As an example of such simulations, von Toussaint et al. [14] used Molecular Dynamics (MD) with Juslin et al. [17] bond order potential (BOP), and found that twist GBs may act as fast transport channels due to the presence of low-activation-energy migration paths, possibly leading to enhanced diffusion rates for hydrogen in the trace impurity limit. Nevertheless, these results are not conclusive since the overall migration depends on the spatial pattern of the fast channels. Zhou et al. [15] performed density functional theory (DFT) calculations and found that vacant spaces (i.e. with large free volume) in symmetrical tilt boundaries can act as trapping centers for hydrogen, with a trapping energy of 1.11 eV comparable to the binding energy of a hydrogen atom to a vacancy (1.41 eV [18], 1.43 eV [19]). Therefore, a strong segregation of hydrogen atoms to GBs was predicted. Recently, Yu et al. [16] calculated diffusion barriers of two possible diffusion paths in a tilt grain boundary using MD with the Li et al. [20] BOP. Their findings indicated that diffusion barriers might be significantly higher than in bulk tungsten and that there is segregation of hydrogen to the grain boundary.

The aim of this paper is to study hydrogen diffusion and trapping in general grain boundaries, rather than special (coincidence site lattice or low-angle) boundaries. For this purpose, we carried out Molecular Dynamics (MD) simulations of hydrogen diffusion in ncW with mean grain size of 5 and 10 nm. Firstly, the diffusion coefficient is calculated as a function of hydrogen concentration in the sample (0.1 at.% < [H] < 10.0 at.%) in the temperature range from 1200 to 2000 K. Secondly, trapping energies of grain boundaries are estimated via the potential energy per hydrogen atom and diffusion results are interpreted within the framework of a trapping model proposed by Kirchheim [21] for nanocrystalline materials. Finally, H–H interaction is evaluated with regard to possible $H_2$ formation, and segregation of hydrogen to GBs is assessed.

## 2. Methods

### 2.1. Simulation methods

MD simulations were performed using LAMMPS [22] and a bond order potential (BOP) [20] for the W–H system. The BOP used in this work is a modified version of Juslin et al. [17] BOP, and provides a better description of defect formation energies. Although values for the diffusion coefficient of hydrogen in bulk W calculated via MD are not reported in that article, static calculations of the diffusion energy barrier (activation energy) are in agreement with those calculated by ab initio techniques (for further discussion on this topic see [23,18,24,25]).

The tracer diffusion coefficient of H in W ($D_s$) can be defined by the Einstein–Smoluchowski equation [26]:

$$D_s = \lim_{t\to\infty} \frac{1}{6t} \left\langle [\mathbf{r}(t) - \mathbf{r}(0)]^2 \right\rangle \tag{1}$$

where the ensemble average is taken over all hydrogen atoms in the system and $\mathbf{r}(t)$ is the position of these atoms at time $t$. $D_s$ can be derived from the slope of the plot $\left\langle [\mathbf{r}(t) - \mathbf{r}(0)]^2 \right\rangle / 6$ vs. $t$. For a single flat tilt and twist GB (see for instance [27]) one could define a diffusivity along the GB plane, and another perpendicular to it. Here we have instead a large collection of GBs which are typically not flat and display more disorder than tilt and twist boundaries. Therefore, Eq. (1) defines a macroscopic magnitude that averages the fine inhomogeneous structure of our nanocrystalline samples, representative thus of the physical volume element. This is akin to the assignment of a scalar diffusivity to untextured polycrystals, though at a much finer scale. As will be shown later on, in our particular case it also allows for a qualitative appreciation of the relative impact of grain boundary and bulk regions on the diffusion process.

Although there is evidence that the temperature dependence of $D_s$ could deviate from an Arrhenius law in amorphous metals [28], it is assumed that, for the limited temperature range studied in this paper, the tracer diffusion coefficient does obeys an Arrhenius law:

$$D_s = D_s^0 \exp(-E_a/k_B T) \tag{2}$$

with $D_s^0$ an exponential pre-factor, and $E_a$ the activation energy.

For the purpose of analyzing the results, it is considered that a site energy can be assigned to each hydrogen atom. A practical way to estimate site energies is calculating the potential energy of each hydrogen atom. As the BOP is a many-body potential, the potential energy per atom is not clearly defined. For the sake of simplicity, the site energy of hydrogen $i$ is calculated as:

$$E_i = \sum_{j\neq i} \frac{1}{2} f^c(r_{ij}) \left[ V^R(r_{ij}) - b_{ij} V^A(r_{ij}) \right]. \tag{3}$$

Here $r_{ij}$ is the distance between atoms $i$ and $j$, $f^c$ is a smooth cutoff function, $V^R$ and $V^A$ are repulsive and attractive pair potentials respectively, and $b_{ij}$ represents a measure of the bond order (i.e. the strength of each bond) and is a nonlinear function of three-body contributions [20]. The advantage of estimating site energies with Eq. (3) rather than with standard binding or formation energy calculations is the saving of computational time. In addition, it was verified that there is a remarkable linear relationship between binding energy and site energy as estimated with Eq. (3).

The binding energy of two hydrogen atoms ($E_b^{\mathrm{HH}}$) is obtained as:

$$E_b^{\mathrm{HH}} = 2E(W_n\mathrm{H}) - [E(W_n\mathrm{H}_2) + E(W_n)] \tag{4}$$

where $E(W_n)$ refers to the energy of the reference bulk W with $n$ atoms, $E(W_n\mathrm{H})$ refers to the reference bulk W with an H atom residing in a tetrahedral interstitial site (TIS), and $E(W_n\mathrm{H}_2)$ is the energy of the reference bulk with two H atoms in different TIS. With this definition, a positive binding energy represents attraction between H pairs.

The hydrogen–vacancy binding energy ($E_b^{HV}$) is defined as:

$$E_b^{HV} = [E(W_{n-1}V) + E(W_n\mathrm{H})] - [E(W_{n-1}VH) + E(W_n)] \tag{5}$$

where $E(W_{n-1}VH)$ is the energy of an H atom in its lowest energy site in a W monovacancy, and $E(W_{n-1}V)$ is the energy of the same system containing a single vacancy. As for Eq. (4) above, a positive value means the H–vacancy pair is more stable than the separated constituents.

### 2.2. Simulated systems

Nanocrystalline W (ncW) samples with grain sizes of 5 and 10 nm were created using an in-house Voronoi tessellation code. Each sample contains 60 randomly oriented grains and is cubic with a box side of 50 and 100 lattice constants respectively. Grain size distribution was calculated and the results can be described by a log–normal distribution with mean $E(X) = 5.027$ nm and $E(X) = 10.083$ nm. This distribution is frequently observed as a result of crystallization processes, especially random nucleation and growth [29].

Simulations were carried out to understand hydrogen behavior in real nanostructured W samples, which contain a large diversity of GBs. Fig. 1 shows a dark field transmission electron microscopy of a pure α-phase nanostructured sample with a thickness of 30 nm deposited by DC magnetron sputtering. More details about fabrication procedure and coatings properties are reported in [30]. In this image, it is observed that the coating is made of grains presenting anisotropic shapes, with sizes between 50 and 150 nm.

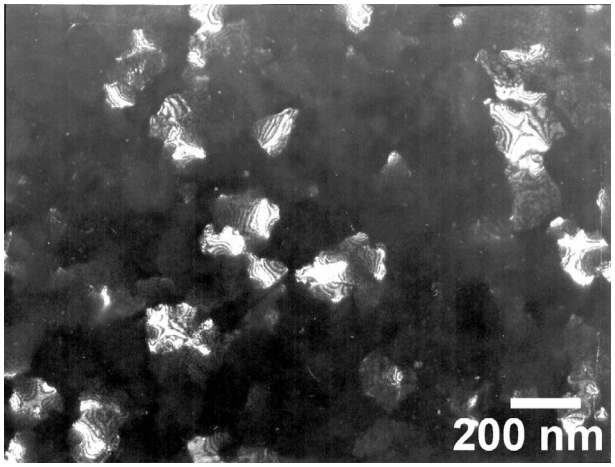


**Fig. 1.** Dark field TEM image of a ncW sample with a thickness of 30 nm obtained with a JEOL JEM 2100 microscope operated at 200 kV.

The high contrast observed between adjacent grains may suggest that GBs are mostly of large-angle type, though some low-angle GBs are also present (low contrast regions). Furthermore, it is known that the Voronoi construction used to create the *simulated* nanocrystalline samples produces mostly high-angle GBs [31]. Therefore, in spite of the difference in grain size between the simulated and experimental samples, both have in common a large fraction of high-angle GBs.

The potential energy of the simulated samples was minimized and subsequently an annealing was performed in the NPH/isokinetic ensemble for 100 ps at 2000 K while the pressure was kept at zero. The heating and cooling rate were 1000 K/ps and 200 K/ps respectively. The reason for a lower cooling than heating rate is that it was verified that a lower potential energy was achieved with a slow cooling. All simulations were carried out with an integration time step of 1 fs.

The porosities of the samples after relaxation relative to the density of the crystalline phase ($1 - \rho/\rho_{\text{bulk}}$) were 2.1% and 1.2% for the 5 and 10 nm samples, respectively. Similarly, the respective fractions of GBs, as calculated with common neighbor analysis (CNA) [32] technique, were 42.4% and 22.5%.

Hydrogen was introduced in the samples by three different methods: (a) using random positions uniformly distributed in the sample's volume, (b) identifying W atoms in GBs by means of CNA and switching a suitable number of them to hydrogen atoms, and (c) calculating the Voronoi volumes (the volume of the Wigner–Seitz cell) of W atoms [33] and placing the hydrogen atoms in a random fashion within the largest Voronoi volumes. $D_s$ was found to depend on the hydrogen insertion method. Assuming that hydrogen segregates towards GBs, insertion methods (b) and (c) are preferred since they give rise to closer to equilibrium configurations. However, insertion method (b) produces substantial alteration of the microstructure in addition to changing the number of W atoms in the samples. Hence, the Voronoi insertion method (c) emerges as the most appropriate one for performing simulations. Furthermore, inserting hydrogen atoms in the largest Voronoi volumes is justified on the grounds that these are regions of charge density depletion, and since the charge density in GBs is greater than the optimal density, hydrogen exhibits the lowest energy where the charge density depletion is largest, i.e. largest Voronoi volumes [15]. After hydrogen insertion, further minimization and annealing were carried out. The parameters used were the same as for the prior annealing, with exception of time and cooling rate (10 ps and 1000 K/ps, respectively).

As illustrated in Table 1, samples with different hydrogen concentrations (0.1 at.% < [H] < 10.0 at.%) were created. Additional samples with 20 at.% and 30 at.% of hydrogen were constructed but they were neglected for $D_s$ calculations since in these samples an increase in grain boundary fraction, as identified by CNA, was observed. Nonetheless, the latter samples were used to study H–H interaction. Fig. 2 shows a cross-section of the 5 nm sample after 1 at.% hydrogen insertion.

**Table 1**
Simulated samples and results of fitting diffusion coefficient data to the Arrhenius law.

| Structure | $d$ (nm) | C (at.% H) | $D_s^0$ ($\times 10^{-8}$ m$^2$/s) | $E_a$ (eV) |
|---|---|---|---|---|
| nc | 5 | 10 | 13 ± 2 | 0.70 ± 0.03 |
| nc | 5 | 1 | 6 ± 2 | 0.71 ± 0.05 |
| nc | 5 | 0.5 | 6 ± 3 | 0.74 ± 0.06 |
| nc | 5 | 0.1 | 2 ± 0.4 | 0.65 ± 0.02 |
| nc | 10 | 1 | 11 ± – | 0.77 ± – |
| bulk | – | 1 | 5 ± 1 | 0.20 ± 0.04 |
| bulk | – | 0.1 | 4 ± 1 | 0.17 ± 0.04 |

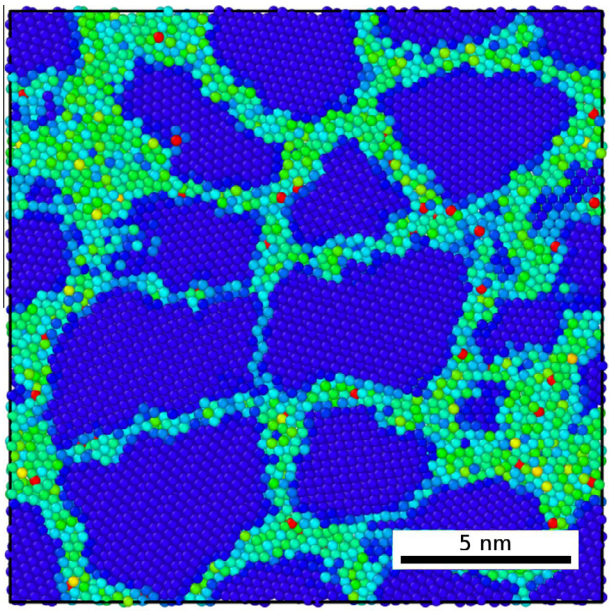


**Fig. 2.** Cross-section of the 5 nm sample with 1 at.% hydrogen in grain boundaries. W atoms colored coded with centro-symmetry parameter and H atoms in red. Obtained with OVITO [51]. (For interpretation of the references to color in this figure legend, the reader is referred to the web version of this article.)

The diffusion coefficient was calculated using Eq. (1) in the same ensemble used for annealing. The mean square displacement was calculated every 0.1 ps and for a total time of 30 ps approximately. For samples with low concentrations and temperatures (e.g. 0.1 at.% H and 1200 K), the simulation time was extended up to 80 ps to avoid excessive fluctuations of $D_s$.

Bulk diffusivity calculations were performed in the same way. The configurations employed for hydrogen concentrations of 0.1% and 1% consisted of cubic boxes with 31,250 and 54,000 W atoms, respectively. Hydrogen was introduced randomly in the simulation box with uniform probability.

## 3. Results

The diffusion coefficient was calculated for all samples at five different temperatures: 1200 K, 1400 K, 1600 K, 1800 K, and 2000 K. It is worthwhile to mention that because of the high computational cost only two $D_s$ values were calculated for the 10 nm sample. Fig. 3 shows the calculated diffusion coefficients and the

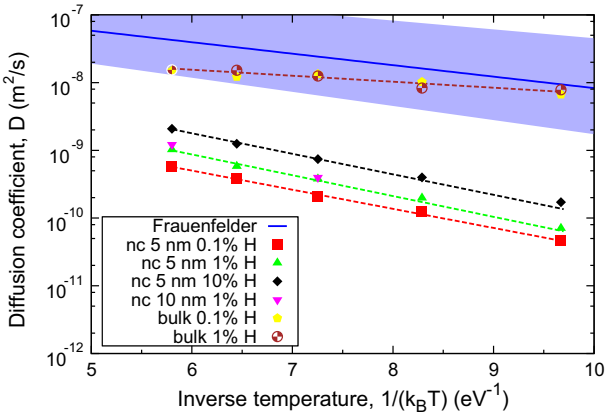


**Fig. 3.** Calculated diffusion coefficients (colored symbols) and Arrhenius fit (dashed lines) for bulk and nanocrystalline samples. The continuous blue line corresponds to the results reported by Frauenfelder [34]. The shaded area indicates the uncertainty region for the experimental results. (For interpretation of the references to color in this figure legend, the reader is referred to the web version of this article.)

Arrhenius fit (lines) for bulk and nanocrystalline samples, together with the experimental values determined by Frauenfelder [34] ($D_s^0 = 4.1^{+5.0}_{-2.0} \times 10^{-7}$ m$^2$/s, $E_a = 0.39 \pm 0.09$ eV). Results obtained from fitting the data to Eq. (2) are listed in Table 1 together with their corresponding errors.

To characterize H–H interaction, pair distribution functions for hydrogen atoms were obtained for all the studied samples. Results for bulk samples did not show significant interaction, within the empirical potential cut-off, for any of the studied concentrations.

Histograms of site energies for hydrogen atoms were obtained by means of Eq. (3) after quenching to 20 K. Comparison between histograms of site energy for different hydrogen concentrations and grain sizes is performed in Fig. 4 to illustrate the effects of the various parameters.

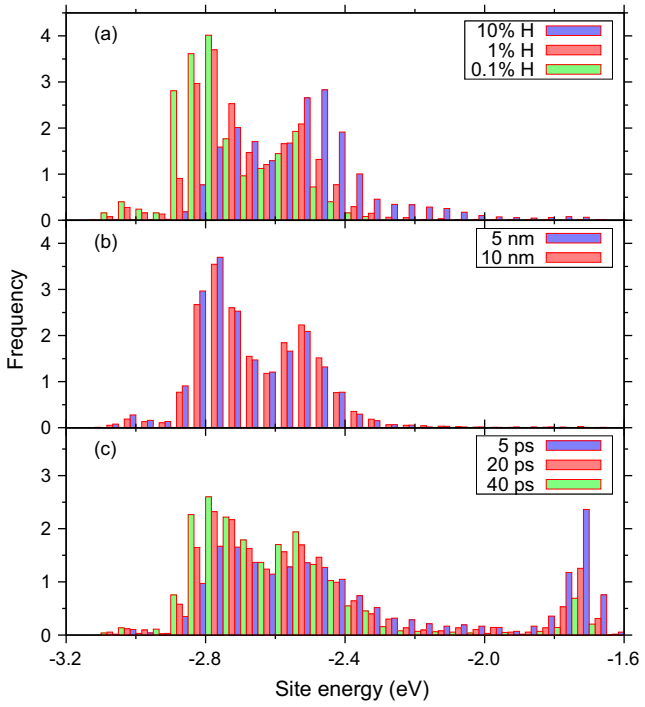


**Fig. 4.** Histograms of site energies for different: (a) hydrogen concentrations (5 nm, 20 K), (b) grain sizes (1 at.%H, 20 K), and (c) quenching times (5 nm, 20 K, random inserted 1 at.%H).

In order to study segregation, hydrogen was randomly introduced in the 5 nm nc sample with a uniform probability distribution. Subsequently the sample was annealed at 2000 K and then quenched at regular periods. Fig. 4c shows histograms of site energies at 20 K of samples quenched at different times (5 ps, 20 ps, and 40 ps).

## 4. Discussion

### 4.1. Diffusion coefficient

The calculated diffusion coefficient ($D_s$) of hydrogen is lower in ncW than in bulk W by at least one order of magnitude in the temperature range 1200–2000 K (Fig. 3). Furthermore, as shown in Fig. 3, the diffusion coefficient in ncW increases with rising hydrogen concentration, whereas in bulk W it does not depend on concentration, at least below 1 at.% H. These results are in agreement with experimental findings in other nc metals [35], although in this work an enhanced diffusion above a certain concentration threshold is not found. From this data, it may be concluded that diffusion of hydrogen in ncW is trap dominated, and that GBs do not provide high diffusivity paths for hydrogen (in accordance with other studies [36–38] and in disagreement with those data reported by von Toussaint et al. [14]). The reason for such discrepancy might be due to the fact that, as a consequence of the construction process of the ncW samples employed in this work, we are dealing with high energy or out of equilibrium GBs.

A rough analysis also shows that H diffusion mainly takes place through the (relatively thick) GB regions as opposed to the bulk-like ones. For the diffusivity we may set approximately,

$$D = f_{\text{bulk}} D_{\text{bulk}} + f_{\text{GB}} D_{\text{GB}} \tag{6}$$

where $f_X/D_X$ refer to the statistical weight/diffusivity of H in region X. By putting $f_{\text{bulk}} \propto 1$, we get $f_{\text{GB}} \propto \exp(E_B/kT)$, but for a non-essential factor, where $E_B$ is some representative binding energy of H to the GBs. Moreover, from Fig. 4 the average site energy of H in GBs can be obtained and the corresponding binding energy is estimated to be $E_B \approx 2$ eV using Table 2; consequently $f_{\text{GB}} \gg f_{\text{bulk}}$ (trapping and segregation effects are also discussed later). Thus, the predicted activation energy for the 1st term of Eq. (6) would be (cf. Table 1) $E_{\text{bulk}} \approx 0.2 + 2.0 = 2.2$ eV, which is sizably larger than the calculated 0.7 eV for the whole D. In summary, the above relationship, in the investigated temperature range, is dominated by the 2nd term.

Additionally, the diffusion coefficient calculated for the 10 nm sample with 1 at.% H exhibits no significant difference from the one obtained for the 5 nm sample with the same H concentration. This behavior, as discussed in Section 4.2, is related to the concentration of hydrogen at GBs.

Finally, it is worth to highlight the similarities between the results from this work and that reported by Lee and Lee [39] for a Cu–Zr bulk metallic glass (BMG). They also found a lower $D_s$ in the BMG than in the crystalline phase, and a strong dependence of $D_s$ on hydrogen concentration, suggesting that the nanocrystals constructed in this work can be described, for the purpose of diffusion, as a heterogeneous system with both ordered and disordered phases. This view has also been used to explain mechanical

**Table 2**
Comparison between site energies ($E_i$) and binding energies ($E_b^{MD}$) calculated in this work. DFT results ($E_b^{DFT}$) are shown for reference.

| Site | $E_i$ (eV) | $E_b^{MD}$ (eV) | $E_b^{DFT}$ (eV) |
|---|---|---|---|
| bulk | −1.71 | 0.0 | 0.0 |
| vacancy | −2.59 | 2.03 | 1.41 [18], 1.43 [19] |

properties of nanocrystals [7], with slightly different results depending on nanocrystal construction details [40,41].

### 4.2. Trapping

Trapping is one of the main processes controlling retention of hydrogen isotopes in tungsten. In order to understand experiments, it is important to determine which microstructural defects are involved in the trapping process and their related trapping energies. Trapping energies ($E_t$) are usually approximated as the sum of the binding energy ($E_b$) and the migration barrier ($E_m$) of the fastest particle [19]. For reference, site energies calculated with Eq. (3), binding energies calculated with Eq. (5), and binding energies obtained with Density Functional Theory (DFT) calculations are given in Table 2 for an H atom in bulk W and in a distorted octahedral site in a monovacancy.

As shown in Fig. 4, GBs in ncW samples present a site energy distribution centered at −2.6 eV, which is approximately the site energy of an H atom in a vacancy (see Table 2). The main conclusion is that traps in "general" GBs may present a broad distribution of trapping energies centered at the vacancy trapping energy. This suggests that traps in GBs are free volume related, and that the result of Zhou et al. [15] for a symmetrical tilt grain boundary, where the deepest traps have lower trapping energy than for the vacancy, might be a feature of that particular boundary, but not a general behavior. The fact that GB trapping energies may be similar to the vacancy trapping energy has been suggested by Anderl et al. [42]. Ogorodnikova et al. [13] conjectured that trap energies of 0.85 eV could be related to native defects, including GBs. We foresee that the origin of this discrepancy is mainly related to the impossibility to separate the contribution of GBs from that of other native and ion-induced defects in real experiments. Indeed, this value is closer to that calculated by Terentyev et al. [43] using DFT for dislocation trapping (∼ 0.55 eV), than to our value associated to GBs. The trapping energy of hydrogen isotopes to a vacancy has been reported by several authors to be ∼ 1.4 eV [12,13,44].

The diffusion results previously described can be understood within the trapping model proposed by Kirchheim [21], which assumes that the distribution (thermal occupation) of hydrogen atoms among the different sites present in GBs and bulk can be described by Fermi–Dirac statistics. Thus, each site is allowed to be occupied by one or zero hydrogen atoms. Sites in the bulk have a well defined energy while those in the GBs present a site energy distribution. Regarding diffusion, Kirchheim's central assumption is that *on average* the diffusion barrier is smaller for high energy sites than for low energy ones. In other words, when a hydrogen atom is occupying a high energy site its jump probability increases, leading to a higher diffusivity.

The calculated dependence of the diffusion coefficient on hydrogen concentration and grain size are explained with this model as follows. Fig. 4a shows that with increasing hydrogen concentration, higher energy sites become occupied and thus, the average diffusion barrier is diminished, explaining the increase in diffusivity observed in Fig. 3. In contrast, site occupation is not altered significantly with increasing grain size at constant global hydrogen concentration, as seen in Fig. 4b. The reason of this behavior is that, assuming complete segregation, hydrogen concentration in GBs is only doubled when increasing the grain size from 5 to 10 nm (since the fraction of GBs is halved) whereas changes in concentration in Fig. 4a span two orders of magnitude (0.1 at.% < [H] < 10.0 at.%). Hence, the simulated grain size range is insufficient to determine the diffusion coefficient dependence on grain size.

Kirchheim [21,28,35] derived an expression for the tracer diffusion coefficient in nanocrystalline materials based on transition state theory and the assumptions of constant saddle point energy, and Gaussian distribution of GB energies (see Appendix A). As these

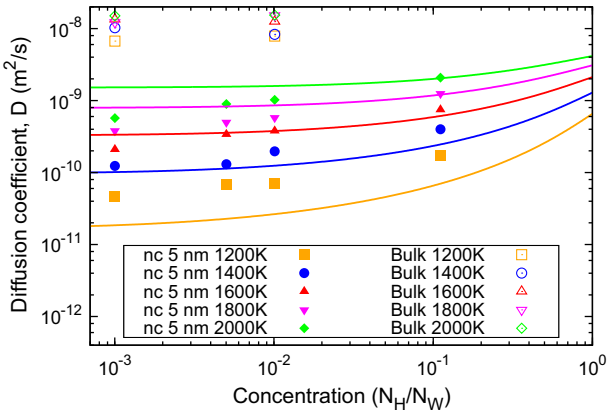


**Fig. 5.** Concentration dependence of the calculated diffusion coefficients for bulk and nanocrystalline samples. Predictions from Kirchheim's model [21] are shown with continuous lines for nanocrystalline samples.

hypothesis are only partially fulfilled in the systems simulated in this paper, only a semi-quantitative agreement can be expected. In order to check the validity of these hypothesis, Eq. (A.3) was fitted to the MD data via the mean ($E_1$) and standard deviation ($\sigma$) of the Gaussian distribution corresponding to grain boundary energies. Values for the bulk diffusion coefficient ($D_0$ and $E_a$) were taken from Table 1 (bulk 1 at.% H), $c_t$ was calculated with common neighbor analysis to be almost 0.4, and $E_0 = 0.86$ eV was employed for bulk sites energy as reported in [20]. Since reasonable agreement could not be obtained for all temperatures, a higher weight in Eq. (A.4) was given to the intermediate temperature, i.e. 1600 K. The results obtained from the fitting procedure outlined in Appendix A were $E_1 = 0.58 \pm 0.01$ eV and $\sigma = 0.43 \pm 0.01$ eV. Fig. 5 shows the dependence of the diffusion coefficient with concentration as obtained from our MD simulations and the prediction with Eq. (A.3). The agreement found is fair, given the simplicity of the model, and captures the essential features of the concentration and temperature dependence. Unfortunately, the difference between bulk sites energy ($E_0$) and the mean of the Gaussian distribution ($E_1$), i.e. $E_0 - E_1 = 0.28$ eV, does not seem consistent with Fig. 4. It is asserted that this inconsistency arises due to the already discussed simplicity of the model.

From our studies, we observe that each grain boundary atom in the H free sample can accommodate at least a single H atom. This is consistent with the peak at 0.17 nm in the H radial distribution function discussed in Section 4.3. It has been seen that a single vacancy can trap up to 6–10 H atoms without leading to H molecule formation and possible interstitial emission [45]. Therefore, a single H atom in each W atom in GBs is a reasonable lower limit to H trapping. We could extrapolate from the 5 nm nanograined sample to a sample with grain size $d = 5$ μm by assuming that the relationship between grain boundary atoms and atoms inside the grain goes as $\sim 1/d$. Therefore, the amount of H which can be retained by GBs in such sample would be around 0.035 at.% H. Neglecting GBs and assuming an extremely high dislocation density of $10^{12}$ $1/m^2$, we can estimate H retention using the estimate by Terentyev et al. [43], where a dislocation segment of 0.275 nm can accommodate 6 H, resulting in approximately 0.000035 at.% H retention. Of course these are rough estimates, given that GB topology will change as H content increases and that we are neglecting H bubble formation, but they point to the relevance of GBs as H trapping sites.

### 4.3. H–H interaction

In order to understand hydrogen behavior in nanostructured W it is very important to determine if molecular hydrogen is formed.

There is no evidence for $H_2$ formation in the samples studied here, even at the largest simulated concentrations (30 at.%). Almost all hydrogen atoms are separated by distances larger than the empirical potential cut-off (0.17 nm). We tracked pairs separated by smaller distances and found that their motion was not correlated, and that inter-H distance increased significantly with time, clearly indicating lack of molecule formation. These results are consistent with DFT results, which show no $H_2$ formation for up to 10 H bonded to a single vacancy [45]. Several articles [46,47,23,48] have found, using DFT calculations, that H–H interaction is mostly repulsive, with a weak attraction for a separation between H atoms at around 0.22 nm, i.e. a distance much longer than the equilibrium distance for an isolated $H_2$ molecule, which is 0.07 nm [20]. Therefore, self-trapping through $H_2$ formation seems to be impossible.

At high H concentrations, the pair distribution function for H in the nc samples at 20 K shows a well-defined peak at 0.17 nm. This might be related to an effective long-range interaction mediated by strain. Binding energy calculations of H–H pairs in bulk W with Eq. (4) (with $n = 2000$) indeed show a weak ($\sim -0.1$ eV) effective repulsive interaction, with a minimum at 0.17 nm (this result was also found in a recent article [49]), in disagreement with DFT calculations cited above. However, diffusion results presented here are not affected by this discrepancy: the fact that $D_s$ in bulk W is independent of concentration indicates that H–H interaction for the concentrations studied is small enough not to alter the diffusion process, and it can be concluded that the dependence of the diffusion coefficient with concentration for nc samples arise solely from the microstructure present in these samples.

### 4.4. Segregation

It is well known that hydrogen tends to segregate in native defects like GBs, possibly changing the mechanical properties of the material. As shown in Fig. 4c there is a strong peak at $-1.71$ eV that corresponds to tetrahedral sites in bulk W and a broad distribution centered at $\sim -2.60$ eV that corresponds to GB sites. As the sample is annealed for longer times the peak at $-1.71$ eV looses intensity, whereas the peak centered at $-2.60$ eV increases, indicating that hydrogen atoms gradually migrate to GBs during annealing. This result suggests that GBs act as strong trapping centers and can lead to intense segregation as predicted by Zhou et al. [15] based on DFT calculations and by Gonzalez-Arrabal et al. [50] by analyzing the hydrogen depth distribution in ncW using resonance nuclear reaction analysis. It must be emphasized that hydrogen segregation to GBs was complete in all simulations performed in this work, as shown in Fig. 4. Finally, it should be noticed that the binding energy of an H atom to a vacancy calculated here with MD overestimates ab initio calculations, as shown in Table 2. Therefore, segregation is probably overestimated by this empirical potential.

## 5. Conclusions

Hydrogen diffusion and trapping in nanocrystalline tungsten with mean grain size of 5 and 10 nm was calculated using Molecular Dynamics (MD). The hydrogen diffusivity calculated for all samples was lower than that reported for coarse-grained tungsten and depends strongly on hydrogen concentration (0.1 at.% < [H] < 10.0 at.%), rising with increasing concentration. Such dependence arises solely from the nanocrystalline structure since it was not observed for bulk tungsten samples, and could be rationalized using Kirchheim's model [21]. One important thing to be considered is the possibility of $H_2$ formation which might affect diffusion. Therefore, H–H interaction was evaluated, disregarding the possible formation of $H_2$.

Grain boundary trapping energies were estimated and a broad distribution roughly centered at the vacancy trapping energy was found, giving trapping energies which are higher than those previously calculated for special GBs in bycristals [15]. In addition, for typical polycrystals, the amount of hydrogen which can be retained in grain boundaries was estimated to be significantly larger than the amount which can be retained in dislocations. Finally, segregation of hydrogen towards grain boundaries was studied by annealing the 5 nm sample at 2000 K and quenching at regular periods, resulting in hydrogen preferential migration towards grain boundaries during annealing, and also supporting grain boundaries as strong trapping sites.

In conclusion, these results contribute to the understanding of hydrogen behavior in polycrystalline tungsten, which is a strong candidate as first wall material in nuclear fusion reactors. Nevertheless, in order to arrive at definite conclusions about material performance, a more complete understanding of the hydrogen impact on the material properties is needed, including the role of hydrogen in the mechanical properties of the material, the role of radiation-induced defects as competing trapping sites, etc.

## Acknowledgements

We thank K. Nordlund for providing the potential tables. PMP thanks support from a scholarship from the Comisión Nacional de Energía Atómica (CNEA); EMB thanks support from PICT2009-0092 (Argentina) and a SeCTyP-UNCuyo grant. RCP thanks PIP 804/10 CONICET for partial support. Research by NG is supported by MINECO (Spain) under project JdC-2012. Part of the work was financed by MINECO (Spain) under project MAT2012-38541-C02-01.

## Appendix A. Trapping model

In this appendix we summarize the assumptions and equations involved in applying the model proposed by Kirchheim [21] to explain diffusivity in nanocrystalline metals. Throughout the appendix, concentrations ($C$) are expressed as the ratio of hydrogen atoms ($N_H$) to interstitial sites ($N$), i.e. $C = N_H/N$. These are then converted to the ratio of hydrogen atoms to matrix atoms ($N_{\text{matrix}}$), i.e. $c = N_H/N_{\text{matrix}}$, multiplying by the number of interstitial sites per matrix atom ($\beta$) such that $c = \beta C$. $\beta$ is supposed to be constant, disregarding disorder in grain boundaries, and is taken as 6 for bcc structures.

The model assumes that hydrogen atoms are distributed according to Fermi–Dirac statistics in interstitial sites of a matrix atomic structure (bulk and grain boundaries). There are fractions $c_t$ and $(1 - c_t)$ of matrix atoms belonging to grain boundaries and bulk, respectively. Bulk sites are all equivalent, with a well defined energy $E_0$ (an energy reference immaterial to the results), and grain boundary sites follow a Gaussian distribution of energies with mean $E_1$ and standard deviation $\sigma$. The total distribution function is then [35]:

$$n(E) = (1 - c_t)\delta(E - E_0) + \frac{c_t}{\sigma\sqrt{\pi}} \exp\left[\left(\frac{E - E_1}{\sigma}\right)^2\right]. \tag{A.1}$$

Concentrations can be obtained multiplying Eq. (A.1) by the Fermi–Dirac distribution and integrating with respect to $E$:

$$C(\mu) = \frac{1 - c_t}{1 + \exp\left(\frac{E_0 - \mu}{k_b T}\right)} + \frac{c_t}{\sigma\sqrt{\pi}} \int_{-\infty}^{\infty} \frac{\exp\left[\left(\frac{E - E_1}{\sigma}\right)^2\right]}{1 + \exp\left(\frac{E - \mu}{k_b T}\right)} dE. \tag{A.2}$$

where $\mu$ is the chemical potential. Eq. (A.2) must be solved numerically and inverted to obtain $\mu = \mu(C)$.

An expression for the tracer diffusion coefficient ($D_s$) can be derived under the framework of transition state theory, and assuming constant vibrational frequencies and constant saddle point energy. $D_s$ is then given by [28]:

$$D_s(C) = D_s(\text{bulk}) \exp\left(\frac{\mu(C) - E_0}{k_b T}\right) \frac{(1-C)^2}{C} \tag{A.3}$$

This equation is also applicable for the nanostructured samples considered here, as previously discussed for Eq. (1).

In order to apply the model to our simulation results, the following objective function ($\xi$) was minimized:

$$\xi(E_1, \sigma) = \sum_{T,\,C} w(T) \left[\ln\left(D_s^{\text{data}}\right) - \ln\left(D_s^{\text{model}}\right)\right]^2 \tag{A.4}$$

where $D_s^{\text{data}}$ are the diffusion coefficients calculated via MD, $D_s^{\text{model}}$ are the diffusion coefficients calculated with Eq. (A.3), and $w(T)$ are weights given to each temperature. A grid was constructed in the $E_1 - \sigma$ space, and $\xi(E_1, \sigma)$ was calculated for each point in the grid. Finally, careful analysis of the domain allowed identification of regions where $\xi$ presents minima.

## References


[1] V. Barabash, G. Federici, R. Matera, A.R. Raffray, I.H. Teams, Phys. Scripta T81 (1999) 74.
[2] J. Alvarez, A. Rivera, R. Gonzalez-Arrabal, D. Garoz, E. del Rio, J.M. Perlado, Fusion Sci. Technol. 60 (2011) 565.
[3] J. Alvarez, R. Gonzalez-Arrabal, A. Rivera, E.D. Rio, D. Garoz, E. Hodgson, F. Tabares, R. Vila, M. Perlado, Fusion Eng. Des. 86 (2011) 1762.
[4] W. Wang, J. Roth, S. Lindig, C. Wu, J. Nucl. Mater. 299 (2001) 124.
[5] M. Rieth, S. Dudarev, S.G. de Vicente, et al., J. Nucl. Mater. 442 (2013) S173.
[6] S. Wurster, R. Pippan, Scripta Mater. 60 (2009) 1083.
[7] M. Meyers, A. Mishra, D. Benson, Prog. Mater. Sci. 51 (2006) 427.
[8] X.-M. Bai, A.F. Voter, R.G. Hoagland, M. Nastasi, B.P. Uberuaga, Science 327 (2010) 1631.
[9] G. Ackland, Science 327 (2010) 1587.
[10] M. Aucouturier, J. Phys. Colloq. 43 (1982) C6–175.
[11] Y. Ueda, H. Kashiwagi, M. Fukumoto, Y. Ohtsuka, N. Yoshida, Fusion Sci. Technol. 56 (2009) 85.
[12] R.A. Causey, J. Nucl. Mater. 300 (2002) 91.
[13] O. Ogorodnikova, J. Roth, M. Mayer, J. Nucl. Mater. 313–316 (2003) 469.
[14] U. von Toussaint, S. Gori, A. Manhard, T. Höschen, C. Höschen, Phys. Scripta T145 (2011) 014036.
[15] H.-B. Zhou, Y.-L. Liu, S. Jin, Y. Zhang, G.-N. Luo, G.-H. Lu, Nucl. Fusion 50 (2010) 025016.
[16] Y. Yu, X. Shu, Y.-N. Liu, G.-H. Lu, J. Nucl. Mater. 455 (2014) 91.
[17] N. Juslin, P. Erhart, P. Traskelin, J. Nord, K.O.E. Henriksson, K. Nordlund, E. Salonen, K. Albe, J. Appl. Phys. 98 (2005) 123520.
[18] D.F. Johnson, E.A. Carter, J. Mater. Res. 25 (2010) 315.
[19] K. Heinola, T. Ahlgren, K. Nordlund, J. Keinonen, Phys. Rev. B 82 (2010) 094102.
[20] X.-C. Li, X. Shu, Y.-N. Liu, F. Gao, G.-H. Lu, J. Nucl. Mater. 408 (2011) 12.
[21] R. Kirchheim, Acta Metall. 30 (1982) 1069.
[22] S. Plimpton, J. Comput. Phys. 117 (1995) 1.
[23] Y.-L. Liu, Y. Zhang, G.-N. Luo, G.-H. Lu, J. Nucl. Mater. 390–391 (2009) 1032.
[24] K. Heinola, T. Ahlgren, J. Appl. Phys. 107 (2010) 113531.
[25] Y.-L. Liu, W. Shi, Fusion Eng. Des. 88 (2013) 368.
[26] H. Wipf, Diffusion of hydrogen in metals, in: H. Wipf (Ed.), Hydrogen in Metals III, Topics in Applied Physics, vol. 73, Springer, Berlin Heidelberg, 1997, pp. 51–91.
[27] Y. Mishin, M. Asta, A. Vignesh, Acta Mater. 58 (2010) 1117.
[28] R. Kirchheim, U. Stolz, Acta Metall. 35 (1987) 281.
[29] R.B. Bergmann, A. Bill, J. Cryst. Growth 310 (2008) 3135.
[30] N. Gordillo, M. Panizo-Laiz, E. Tejado, I. Fernandez-Martinez, A. Rivera, J. Pastor, C.G. de Castro, J. del Rio, J. Perlado, R. Gonzalez-Arrabal, Appl. Surf. Sci. 316 (2014) 1.
[31] H. Van Swygenhoven, A. Caro, D. Farkas, Mater. Sci. Eng.: A 309–310 (2001) 440.
[32] J.D. Honeycutt, H.C. Andersen, J. Phys. Chem. 91 (1987) 4950.
[33] C.H. Rycroft, Chaos 19 (2009) 041111.
[34] R. Frauenfelder, J. Vac. Sci. Technol. 6 (1969) 388.
[35] T. Mutschele, R. Kirchheim, Scripta Metall. 21 (1987) 135.
[36] J. Yao, J. Cahoon, Acta Metall. Mater. 39 (1991) 119.
[37] A. Pedersen, H. Jonsson, Acta Mater. 57 (2009) 4036.
[38] J.-H. Shim, W.-S. Ko, J.-Y. Suh, Y.-S. Lee, B.-J. Lee, Met. Mater. Int. 19 (2013) 1221.
[39] B.-M. Lee, B.-J. Lee, Metall. Mater. Trans. A 45 (2014) 2906.
[40] D. Wolf, V. Yamakov, S. Phillpot, A. Mukherjee, H. Gleiter, Acta Mater. 53 (2005) 1.
[41] H. Van Swygenhoven, J. Weertman, Mater. Today 9 (2006) 24.
[42] R. Anderl, D. Holland, G. Longhurst, R. Pawelko, C. Trybus, C. Sellers, Fusion Technol. 21 (1992) 745.
[43] D. Terentyev, V. Dubinko, A. Bakaev, Y. Zayachuk, W.V. Renterghem, P. Grigorev, Nucl. Fusion 54 (2014) 042004.
[44] M. Poon, A. Haasz, J. Davis, J. Nucl. Mater. 374 (2008) 390.
[45] Y.-L. Liu, Y. Zhang, H.-B. Zhou, G.-H. Lu, F. Liu, G.-N. Luo, Phys. Rev. B 79 (2009) 172103.
[46] K.O.E. Henriksson, K. Nordlund, A. Krasheninnikov, J. Keinonen, Appl. Phys. Lett. 87 (2005) 163113.
[47] K.O.E. Henriksson, K. Nordlund, A. Krasheninnikov, J. Keinonen, Fusion Sci. Technol. 50 (2006) 43.
[48] C. Becquart, C. Domain, J. Nucl. Mater. 386-388 (2009) 109.
[49] G. Bonny, P. Grigorev, D. Terentyev, J. Phys.: Condens. Matter 26 (2014) 485001.
[50] R. Gonzalez-Arrabal, M. Panizo-Laiz, N. Gordillo, E. Tejado, F. Munnik, A. Rivera, J. Perlado, J. Nucl. Mater. 453 (2014) 287.
[51] A. Stukowski, Model. Simul. Mater. Sci. Eng. 18 (2010) 015012.